Eur. Phys. J. D **13**, 71–82 (2001)

THE EUROPEAN PHYSICAL JOURNAL D

EDP Sciences

Sodium MOT collection efficiency as a function of the trapping and repumping laser frequencies and intensities

S.N. Atutov[1,a], V. Biancalana[2], A. Burchianti[2], R. Calabrese[1], S. Gozzini[3], V. Guidi[1], P. Lenisa[1], C. Marinelli[2], E. Mariotti[2], L. Moi[2,b], K. Nasyrov[2,a], and S. Pod'yachev[2,a]

[1] Dipartimento di Fisica Università di Ferrara and INFN, sezione di Ferrara, via Paradiso 12, 44100 Ferrara, Italy
[2] INFM and Dipartimento di Fisica, Università di Siena, via Banchi di Sotto 55/57, 53100 Siena, Italy
[3] Istituto di Fisica Atomica e Molecolare del CNR, via Alfieri 1, 56010 Ghezzano, Pisa, Italy

Received 10 February 2000 and Received in final form 27 July 2000

Abstract. A detailed theoretical and experimental description of a sodium MOT as a function of the pumping and repumping laser frequencies and intensities is given. The effective trapping schemes and the collection efficiency have been experimentally measured and calculated by solving an original 3D model. This model considers the whole bunch of the 32 ground and excited ($P_{1/2}$ + $P_{3/2}$) Zeeman sublevels, the actual trap geometry, the magnetic field intensity and direction, the light polarization, and evaluates both the velocity capture range v_c and the number of trapped particles N. Synergetic and competition mechanisms due to the trapping and repumping lasers have been predicted and experimentally observed. The model simulation has been compared with the results reported in the literature and with those obtained by us and a quite good agreement has been found. The model can be easily adapted to the other sodium isotopes as well as to all the other alkalis.

PACS. 32.80.Pj Optical cooling of atoms; trapping – 42.50.Vk Mechanical effects of light on atoms, molecules, electrons, and ions – 32.60.+i Zeeman and Stark effects

1 Introduction

Cooling and trapping of atoms and ions are nowadays standard techniques in atomic physics experiments. Atom trapping is the preliminary step for new experiments in laser spectroscopy, frequency standards, collision processes, atom optics, BEC, quantum computing, atomic parity violation etc. Neutral atoms can be efficiently trapped in the so called Magneto Optical Trap (MOT), that has been demonstrated for the first time in 1987 by Raab *et al.* [1] and has been made operative with all alkali atoms [2], francium included [3]. MOT makes use of a magnetic field gradient produced by a quadrupole field and of three pairs of circularly polarized, counterpropagating laser beams. They intercept at right angle in the position where the magnetic field is zero and are detuned to the red of the atomic transition. The red detuning causes cooling of the atoms as in optical molasses, while the Zeeman shifts of the levels produces a position dependent force that confines the atoms in the center of the trap. Due to the hyperfine structure of the alkali ground state, repumping is needed to fight optical pumping. Early experiments with MOT were carried out by slowing first an atomic beam to load the trap [1]. The possibility of trapping atoms directly from the low-velocity edge of the Maxwell-Boltzman distribution made the apparatus much simpler [4].

Even if the basic aspects of atom trapping in a MOT are well understood, peculiar behaviors connected to the specific characteristics of the level structure of the trapped atoms and to the possible competition between the Trapping Laser (TL) and the Repumping Laser (RL) deserve further theoretical and experimental analysis. This effort allows one to have a complete map of trapping conditions and, at the same time, to evaluate the collection efficiency. This last issue is important in the frame of an optimization of the collection efficiency aimed at trapping rare isotopes [6] and short living radioactive species [7]. As different trapping schemes may confine atoms at different temperatures [1], another important subject is the analysis of collision processes over an extended range of energies.

As a preliminary step we focus our attention to the ^{23}Na MOT, which has been realized by many groups and can be a valid test of our model. A detailed theoretical and experimental description of the trapping collection efficiency as a function of the pumping and repumping laser frequencies and intensities will be given. The model considers the whole bunch of the 8 ground and 24 excited

[a] *Permanent address*: Institute for Automation and Electrometry, Novosibirsk, Russia.
[b] e-mail: moi@unisi.it

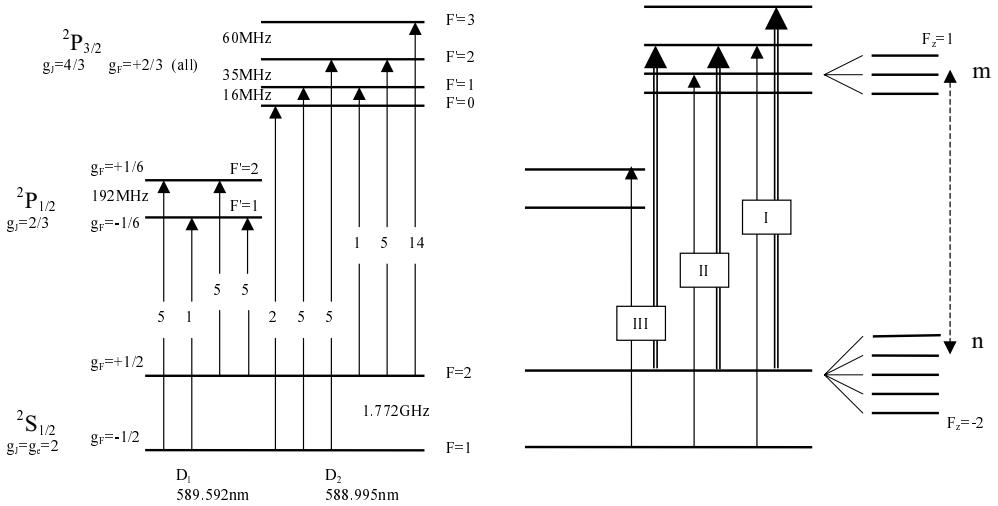

Fig. 1. Fine and hyperfine level structure of sodium D-lines. Oscillator strengths and the Landé factors are reported. The level energy separation is given in frequency units. In the right side, the RL (single arrows) and TL (double arrows) tunings are represented, corresponding to the different trapping conditions discussed in the text, the (m, n) notation used in the theory section is represented as well.

state ($P_{1/2} + P_{3/2}$) Zeeman sublevels (see Fig. 1, where fine and hyperfine structures of the Na D lines are shown), and evaluates both the velocity capture range v_c and the number of trapped particles N.

The theoretical results have been then compared with the experimental ones reported in the literature and with those obtained by us. The model can be easily adapted to the other sodium isotopes as well as to the other alkalis. This is not a trivial result as a detailed analysis of the problem shows that in spite of possible similarities among the alkali hyperfine level structures, relevant differences come out from the specific level separations of each atomic species.

A detailed analysis of the trapping process can be quite complex not only because of the multi-level structure but also because of the simultaneous presence of the trapping and repumping lasers which may show both synergetic and competition effects. In fact, since the first sodium MOT experiment [1], trapping was obtained not only when TL was tuned to the closed $F = 2 \rightarrow F' = 3$ transition but also when it was tuned to the $F = 2 \rightarrow F' = 2$ transition. These two trapping conditions have been named as "type I" and "type II" traps. More precisely, "type I" trap appears when TL is tuned to the red side of the $F = 2 \rightarrow F' = 3$ transition and the RL is tuned to the $F = 1 \rightarrow F' = 2$ transition. "Type II" trap is operative when the laser frequencies are red detuned to the $F = 2 \rightarrow F' = 2$ and $F = 1 \rightarrow F' = 1$ transitions respectively. These configurations are labeled as "I" and "II" in the right side of Figure 1. "Type I" trap produces a cloud of atoms that is more compact and colder than the other one. In fact, according to [1], "type II" trap is two orders of magnitude hotter than "type I" trap. Therefore, even if in the first case the number of trapped atoms is about one order of magnitude smaller than in the second one, the atomic density is higher. This makes "type I" trap the one currently adopted for most applications. "Type II" trap can anyway become interesting if the largest possible number of atoms has to be collected or if "high" temperature collisions are studied. Shang *et al.* [8] stated that "type II" trap is mainly due to the force coming from the $F = 1 \rightarrow F' = 1$ transition. In this case, the "repumping" light works as "trapping" light and the "trapping" laser can be also blue-detuned. This is possible because the $F = 1 \rightarrow F' = 1$ transition is almost a two level closed transition, as 5/6 of excited atoms decay back to the $F = 1$ level of the ground state (consider the branching ratios resulting from the line strength in Fig. 1).

As a matter of fact, the trapping pattern results even more complex after our theoretical and experimental analysis. The adopted apparatus is the standard one with the only peculiarity of making use of two independent dye lasers. This gives us large freedom in the selection of the atomic transitions (both D_1 and D_2), of the laser intensities and frequencies. We found, besides the results reported in the previous experiments, new interesting features well described by our model. In particular by tuning the trapping laser on the D_2 transition and the repumping laser to the D_1 one, we observed two trapping configurations corresponding to a special "type I" and a new "type III" traps (see Fig. 1). "Type III" trap appears only when both lasers are red detuned to the $F = 2 \rightarrow F' = 2$ and $F = 1 \rightarrow F' = 2$ transitions respectively and it disappears as soon as any one of the lasers is blue detuned. Now, as the two $F' = 2$ levels of $P_{1/2}$ and $P_{3/2}$ states have identical lifetimes and branching ratios, the difference between "type II" and "type III" traps is due to the different energy separation among the $F' = 1$ and $F' = 2$ levels of the two P states (see Fig. 1). Therefore the different behavior comes from the fact that in the "type III"

trap no contribution to the trapping force comes from the $F' = 1$ level. Our model gives the right description of this new feature, too. Even if a MOT operating only on the D_1 line has been also observed [9], we do not consider this particular case in the present paper.

2 Theory

A detailed theoretical analysis of a MOT is a hard task because of the complex spatial geometry of the magnetic field, of the changing light polarization with the position, of the possible saturation at high light intensity etc. Our model, which takes into account all the Zeeman sublevels, computes the largest capture velocity and the relative number of atoms that can be trapped. No indication about the final atomic temperature or about the atomic density is given.

2.1 Introduction

The 3D atomic motion in the trap region could be obtained through the numerical solution of the optical Bloch equations of the density matrix of atoms interacting with external e.m. fields [10]. Unfortunately, this approach is not suitable because it requires a huge computing time, due also to the dependence of the force on the e.m. field phases, so that an averaging over a lot of phase configurations is needed to determine the force intensity. These difficulties make interesting the research for a simpler approach. The simplest one considers an atomic model with non-degenerate levels [11,12]. However in this case it is not possible to take into account the effects of the magnetic field and of the e.m. wave polarization that makes the trapping process describable only qualitatively. A more complex model has been proposed by Lindquist *et al.* [13], which consider the effect of the magnetic field and give a more accurate 1D description of the atomic motion, in particular of Cs atoms. However that model neglects the effects induced by the four beams orthogonal to the axis of the coils, which are instead present in the experiment. Moreover as the atom is assumed to be a two level system, this model cannot be used for sodium which has a narrow hyperfine structure of the P states. The main result of this 1D model is that it accounts for the space variation of the magnetic field intensity and direction on the atomic trajectory.

We have developed a 3D model which takes into account the mutual saturation effects of all light beams, the laser polarization, the space dependence of the magnetic field and the Zeeman sublevel mixing due to the Paschen-Back-like effect.

The model describes the capturing process in the MOT of those atoms having an initial velocity

$$v \gg \Gamma/k \tag{1}$$

where Γ is the half line-width and $\mathbf{k}$ is the wave vector. For sodium $\Gamma/k = 3$ m/s and typical velocities of the atoms which can be trapped are $v \cong 10\Gamma/k$. It is important to remark that atoms loose up to 99% of their kinetic energy when condition (1) is satisfied.

In a one-dimensional σ^+–σ^- configuration of two counterpropagating laser beams, the atoms see the two frequencies $\omega_{1,2} = \omega_{\mathrm{L}} \pm kv$, where ω_{L} is the laser frequency. When condition (1) is valid, then $\omega_1 - \omega_2 = 2kv \gg \Gamma$ and the interference effects due to atom interaction with the two laser beams as well as the correlation between the Zeeman sublevels of both excited and ground states can be neglected. Therefore upon the given conditions, the approximation

$$\rho\,(iM|iM') \cong \rho\,(iM|iM')\,\delta_{M,M'} = \rho\,(iM)\,\delta_{M,M'} \tag{2}$$

is valid. Here the indexes i and M define the atomic level and the angular momentum projection on the quantization axis respectively; $\rho\,(iM|iM')$ is the element of the density matrix describing the correlation between two M-sublevels of the i-state; $\rho(iM)$ is the population of the iM state. The assumption of having a diagonal density matrix reduces significantly the number of equations necessary to solve the problem, with respect to the optical Bloch equations. Condition (2) is not valid when $v \ll \Gamma/k$. In this case the correlation between the Zeeman sublevels plays an important role in the generation of polarization gradient forces [14].

Even if the approximation (2) upon the condition (1) has been justified for a 1D trap, its extension to a 3D geometry is not obvious. In fact in the 3D case, for any given reference frame there is always at least one e.m. wave with all polarization components that, at low magnetic field intensity, makes effective the correlation between the Zeeman sublevels. However, as the magnetic field in the trap is zero only in the center and a few Gauss magnetic field can give a Zeeman splitting larger than Γ (in sodium $\Gamma = 5$ MHz and $\mu_{\mathrm{B}} g_{\mathrm{F}} = 1.2$ MHz/G), this problem can be neglected in our context. The polarization components interact with atoms at different effective frequencies in an atomic coordinate system where the quantization axis is coincident with the local external magnetic field direction. This makes possible to neglect the correlation between M-sublevels and use approximation (2) for a 3D trap as well.

2.2 Level population dynamics: the excited levels

The effects of the magnetic field on the Zeeman sublevels of the excited state need an accurate analysis because the interaction energies with the external field in the 10 G range are comparable with the hyperfine interaction. As a consequence an intermediate field Paschen-Back-like approximation is needed and the $|JFM\rangle_H$ basis have to be used instead of the $|JFM\rangle_0$ basis for the zero magnetic field case. The $|JFM\rangle_H$ basis diagonalizes the interaction potential of the electron and nuclear moments and the external magnetic field H. The two bases are correlated through the following linear combination

$$|JFM\rangle_H = \sum_{F_1} c_{FF_1}(M)|JF_1M\rangle_0. \tag{3}$$

Here $c_{FF_1}(M)$ is the unitary matrix consisting in the eigenvectors of the secular equation

$$\sum_{F_1}\langle JFM|V_{HF}|JF_1M\rangle_0\Psi_{F_1} = \Delta E_{JFM}(H)\Psi_F \qquad (4)$$

where the energy shifts $\Delta E_{JFM}(H)$ are given in terms of

$$\hat{V}_{HF} = \mu_{\rm B}\, g_J \mathbf{H}\cdot\hat{\mathbf{J}} + A\hat{\mathbf{J}}\cdot\hat{\mathbf{I}} \qquad (5)$$

that is the interaction potential of the electron moment with the external magnetic field and the nuclear spin. In the following, we will drop off the index H in the $|JFM\rangle$ state notation.

According to the results of this perturbative approach, even at the moderate magnetic field intensities that are typical in the trapping region of a MOT, M-level shifts are not simply proportional to the magnetic field, demonstrating the need for the intermediate-field approximation. We point out that the mixing of M sublevels belonging to different F levels is obtained at magnetic field as weak as a few Gauss, thus making possible the violation of some selection rules, *e.g.* allowing $F = 1 \rightarrow F' = 3$ transition.

2.3 Level population dynamics: rate equations

By keeping valid equation (2) and by making reference to the level notation reported in the right side of Figure 1, the diagonal elements of the density matrix of the new states evolve according to

$$\begin{aligned}\frac{\partial}{\partial t}\rho\left(J_mF_mM_m\right) &= \sum_{s,\sigma} R_{s,\sigma}\left(J_mF_mM_m\right) \\ &\quad - \Gamma_m\,\rho\left(J_mF_mM_m\right) \\ \frac{\partial}{\partial t}\rho\left(J_nF_nM_n\right) &= -\sum_{s,\sigma} R_{s,\sigma}\left(J_nF_nM_n\right) \\ &\quad + \left(\Gamma_m\,\rho\left(J_mF_mM_m\right)\right)_{J_nF_nM_n} \end{aligned} \qquad (6)$$

where Γ_m is the spontaneous decay rate of the m-level, $\left(\Gamma_m\,\rho\left(J_mF_mM_m\right)\right)_{J_nF_nM_n}$ is the population rate of the ground state due to the decay of the excited state, $R_{s,\sigma}\left(J_mF_mM_m\right)$ is the atomic excitation rate to the $|J_mF_mM_m\rangle$ state following photon absorption from the e.m. field s having wave vector $\mathbf{k}_s$ and polarization σ, and $R_{s,\sigma}\left(J_nF_nM_n\right)$ is the ground state depletion rate. These population and depletion rates are given respectively by

$$\begin{aligned} R_{s,\sigma}\left(J_mF_mM_m\right) &= \sum_{F_nM_n} R_{s,\sigma}\left(J_mF_mM_m; J_nF_nM_n\right) \\ R_{s,\sigma}\left(J_nF_nM_n\right) &= \sum_{F_mM_m} R_{s,\sigma}\left(J_mF_mM_m; J_nF_nM_n\right) \end{aligned}$$

with

$$\begin{aligned} R_{s,\sigma}\left(J_mF_mM_m; J_nF_nM_n\right) &= \\ \frac{\Gamma_m}{\hbar^2}&\frac{|\langle J_mF_mM_m|V_{s,\sigma}|J_nF_nM_n\rangle|^2}{\Gamma_m^2/4 + (\omega - \omega_{mn} - \mathbf{k}_s\cdot\boldsymbol{\nu})^2} \\ &\times\left[\rho\left(J_nF_nM_n\right) - \rho\left(J_mF_mM_m\right)\right] \end{aligned} \qquad (7)$$

where, ω_{mn} is the angular frequency of the transition between the $|J_mF_mM_m\rangle$ and $|J_nF_nM_n\rangle$ states, which is given by

$$\omega_{mn} = \frac{E_{J_mF_mM_m}(H) - E_{J_nF_nM_n}(H)}{\hbar}\,. \qquad (8)$$

The hyperfine splitting of the ground state is large enough to allow us to use the Zeeman approximation

$$E_{J_nF_nM_n}(H) = E_{J_nF_n} + \mu_{\rm B} g_{F_n} M_n H \qquad (9)$$

where $E_{J_nF_n}$ is the energy of the unperturbed ground state $|J_nF_n\rangle$ and g_{F_n} is its Landé factor.

2.4 Level population dynamics: matrix elements

In equation (7) $V_{s,\sigma} = -(-1)^\sigma E_\sigma^{(s)} d_{-\sigma}$ is the electric-dipole interaction of the atoms with the wave(s) of σ polarization (with $\sigma = -1,\ 0,\ +1$) and amplitude $E_\sigma^{(s)}$ for the electric field. The matrix element of this potential is

$$\begin{aligned}\langle J_mF_mM_m|V_{s,\sigma}|J_nF_nM_n\rangle &= \\ E_\sigma^{(s)}(-1)^{1+\sigma}&\langle J_mF_mM_m|d_{-\sigma}|J_nF_nM_n\rangle. \end{aligned} \qquad (10)$$

With the help of equation (3), the dipole moment matrix elements can be expressed through the ones at zero magnetic field according to

$$\begin{aligned}\langle J_mF_mM_m|d_\sigma|J_nF_nM_n\rangle &= \\ \sum_{F'_m} c_{F'_mF_m}(M_m)&{}_0\langle J_mF_mM_m|d_\sigma|J_nF_nM_n\rangle. \end{aligned} \qquad (11)$$

By using the Wigner-Eckart theorem and the angular momentum sum rules we have [15]

$$\begin{aligned}{}_0\langle J_mF_mM_m|d_\sigma|J_nF_nM_n\rangle &= (-1)^{F_m-M_m+J_m+J_n+I+1} \\ &\times\left(J_m \parallel d \parallel J_n\right)\sqrt{(2F_m+1)(2F_n+1)} \\ &\times\begin{Bmatrix} J_m & F_m & I \\ F_n & J_n & 1\end{Bmatrix}\begin{pmatrix} F_m & 1 & F_n \\ -M_m & \sigma & M_n\end{pmatrix}. \end{aligned} \qquad (12)$$

Here $\left(J_m \parallel d \parallel J_n\right)$ is the reduced matrix element of the dipole moment for the transition $J_n \rightarrow J_m$ that is connected to the spontaneous decay of the excited state m through the equation

$$\Gamma_m = \frac{4\omega_{mn}^3}{3\hbar c^3}\frac{\left|\left(J_m \parallel d \parallel J_n\right)\right|^2}{2J_m+1}\,. \qquad (13)$$

Holding approximation (2), the ground state population rate by spontaneous emission can be expressed in terms of the electric dipole moments (11)

$$\begin{aligned}\left(\Gamma_m\rho\left(J_mF_mM_m\right)\right)_{J_nF_nM_n} &= \\ \Gamma_m\sum_{\sigma,F_m,M_m}&\frac{|\langle J_mF_mM_m|d_\sigma|J_nF_nM_n\rangle|^2}{\left|\left(J_m \parallel d \parallel J_n\right)\right|^2}\rho\left(J_mF_mM_m\right). \end{aligned} \qquad (14)$$

2.5 Polarisation geometry and evaluation of the force in 3D

It is important to remark that the above equations are written for a coordinate system whose z-axis is coincident with the direction of the magnetic field. As the magnetic field direction changes from point to point along the atomic trajectory, the polarization components of the e.m. wave must be calculated according to the following equation

$$E_{\sigma'} = \sum_{\sigma} D^{1*}_{\sigma,\sigma'}(0,\theta,\phi) E^L_{\sigma} \tag{15}$$

where the E^L_σ are the circular components of the electric field vector in the laboratory frame; $D^1_{\sigma,\sigma'}(0,\theta,\phi)$ are Wigner D-functions, θ and ϕ define the polar and azimuth magnetic field direction angles respectively [16].

Taking into account the meaning of R, the spontaneous force is given by

$$\mathbf{F} = \hbar \sum_{F_m M_m s\sigma} \mathbf{k}_s R_{s,\sigma}(J_m F_m M_m). \tag{16}$$

This gives us a linear system of equations (6, 7, 14) for the density matrix elements $\rho(J_m F_m M_m)$ and $\rho(J_n F_n M_n)$ coupled by optical transitions. The solution of the system allows us to calculate the excitation rates R (Eq. (7)) and the total force $\mathbf{F}$ (Eq. (16)). It is also possible to calculate separately the forces coming from a specific optical transition so to have a detailed analysis of the trap.

2.6 A test of the model

Before to apply our 3D model to the sodium MOT, a test on the simple $J = 1 \rightarrow J = 2$ quantum system has been done. The force calculated with our model has been compared with the one obtained by solving the optical Bloch equations. As an example, in Figure 2 the components of the force acting on an atom in the position (1, 1, 1) with a motion direction (3, 2, 1) in an H-field gradient $\mathrm{d}H_z/\mathrm{d}z = -10$ G/cm are reported as a function of the velocity. A good agreement is found. This allows us to keep valid condition (2) and to apply our solution to the actual Na-MOT.

2.7 Simulation of the trap dynamics

The loading rate of the trap has been calculated as follows: the cooling and trapping region is assumed to be a sphere with a radius equal to that of the laser beam; a particle is trapped if it intersects the surface of this sphere only once. The atomic velocity $\mathbf{v}$ along a given direction $\mathbf{n}$ and with an impact parameter b corresponds to the capture velocity $\mathbf{v}_\mathrm{c}(\mathbf{n}, b)$ if its radial component vanishes at the opposite side of the trapping sphere. Calculations show that for a particle with $\mathbf{v}$ close to $\mathbf{v}_\mathrm{c}(\mathbf{n}, b)$ the trajectory is almost a straight line until it is very close to the edge of the sphere where it is bent. This allows us to calculate $\mathbf{v}_\mathrm{c}$ by using the straight trajectory approximation and a time reversal technique. Namely, we consider particles leaving from any point of the spherical surface with zero velocity and we calculate the motion of the particles back along some given trajectory to the spherical surface where $\mathbf{v}_\mathrm{c}$ is found. Finally, after having checked a very smooth dependence of $\mathbf{v}_\mathrm{c}$ on the direction $\mathbf{n}$, we go on assuming that v_c depends only on b. This procedure allows us to save enormous computing time, by maintaining a satisfactory precision. In this case the flux of trapping atoms is:

$$J = 2\pi \int_0^{r_b} b\,\mathrm{d}b \int_0^{\nu_\mathrm{c}(b)} v^3 f_M(v)\,\mathrm{d}v \tag{17}$$

where

$$f_M(\nu) = \frac{n}{\pi^{3/2} v_\mathrm{T}^3} \mathrm{e}^{-v^2/v_\mathrm{T}^2} \tag{18}$$

is the Maxwell distribution of the atoms in the gas, n is the gas density and v_T is the thermal velocity. The number N

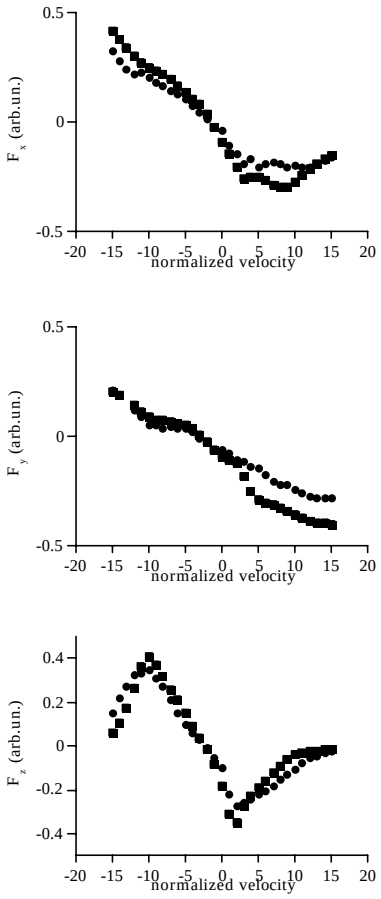

Fig. 2. Components of the radiative forces along the coordinate axis according to the Optical Bloch Equations (•) and to our model (■) in the simple case of a $J = 1 \rightarrow J = 2$ transition. The velocity is expressed in Γ/k units.

of captured atoms is obtained from

$$\frac{\mathrm{d}N}{\mathrm{d}t} = J - \frac{N}{\tau} \tag{19}$$

where τ is the characteristic trap loading time. At steady state regime the number of trapped atoms is $N_{\mathrm{SteadyState}} = \tau J$.

3 Experimental apparatus and results

3.1 Apparatus

The MOT is attained inside a spherical glass cell (diameter about 15 cm) with six flat windows placed along right angle directions, four extra windows are also available for diagnostics. The cell is connected to an ion pump and to a sodium reservoir that is heated up to produce a suitable vapor density, the residual background pressure limits the trap lifetime to about $\tau \cong 1$ s. A pair of coils in anti-Helmoltz configuration gives the quadrupole magnetic field with a field gradient of the order of 10 G/cm; two further coils are used to compensate the H_{earth} and other spurious magnetic fields. Two independent dye lasers have been used in order to check all possible configurations; their beams overlap in the trap region where they are about 1.2 cm in diameter, they are split in three parts along three orthogonal axes and pass trough three quarter-lambda plates producing the suitable circular polarization on each of them. Three mirrors coupled to further quarter-lambda plates reflect the laser beams back in each arm of the trap.

The laser intensities and frequencies are independently settled, with a resolution and stability of few MHz; actually the "trapping" laser TL is an actively stabilized, ring dye laser, while the "repumping" laser RL is an actively stabilized, standing wave dye laser. Two sodium cells are used to set and check both the laser frequencies by saturation spectroscopy technique.

The trapped atoms are detected through the induced fluorescence, allowing for an estimate of the atom number; at the same time a CCD camera detects the cloud size, so that the density can be evaluated as well.

Each of the two lasers could be tuned either to the D_1 and D_2 sodium transitions. Measurements have been made by frequency scanning either the TL or the RL; the two laser intensities can be separately and independently settled as well.

3.2 Frequency scans of the trapping laser, and effects of the laser intensity

As a first general check we have reproduced, tuning both lasers on D_2 lines, the results observed by Raab *et al.* [1] and by Shang *et al.* [8]. Scanning the TL frequency, while the RL frequency was kept fixed to the D_2, $F = 1 \rightarrow F' = 2$ transition we obtained plots like that shown in Figure 3. Figure 3a reports the saturation spectroscopy signal. Figure 3b shows the fluorescence coming from the trap and Figure 3c the model calculation, for a 250 MHz laser frequency scan. Two peaks with different width and intensity appear in the fluorescence signal coming from the MOT (Fig. 3b) that is roughly proportional to the total number of trapped atoms. Those peaks correspond to the mentioned "type I" and "type II" traps. "Type I" trap goes from -40 MHz $< \nu_{\mathrm{TL}} < 0$ MHz detuning, and "type II" trap starts from $\nu_{\mathrm{TL}} < -60$ MHz detuning. Here and in the following, we refer to the detuning with respect to the frequency of the D_2, $F = 2 \rightarrow F' = 3$ transition. The peak corresponding to trap II is larger and more intense than that of peak I. This means, as reported in previous papers, that the number of trapped atoms is larger for trap II than for trap I. This spectrum is well reproduced by the computer simulation (Fig. 3c). Shang *et al.* (Fig. 3 of Ref. [8]) report a similar result. We stress that our experimental condition is different from the one of Raab and Shang experiment [1,8], where the repumping frequency is obtained from an EOM, so that TL and RL are simultaneously scanned.

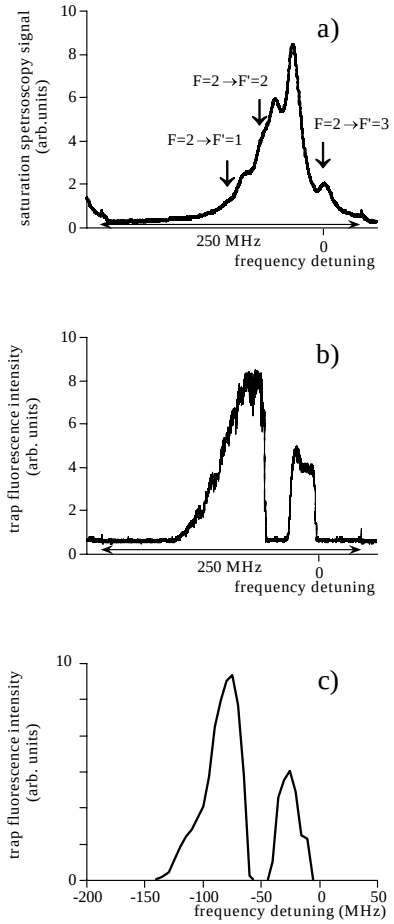

Fig. 3. (a) Saturation spectroscopy signal of the trapping laser (scanning over the D_2 line); (b) fluorescence signal of trapped atoms as a function of trapping laser frequency; (c) fluorescence signal according to the model simulation. The RL is detuned 140 MHz to the red of the nominal D_2, $F = 1 \rightarrow F' = 3$ resonance.

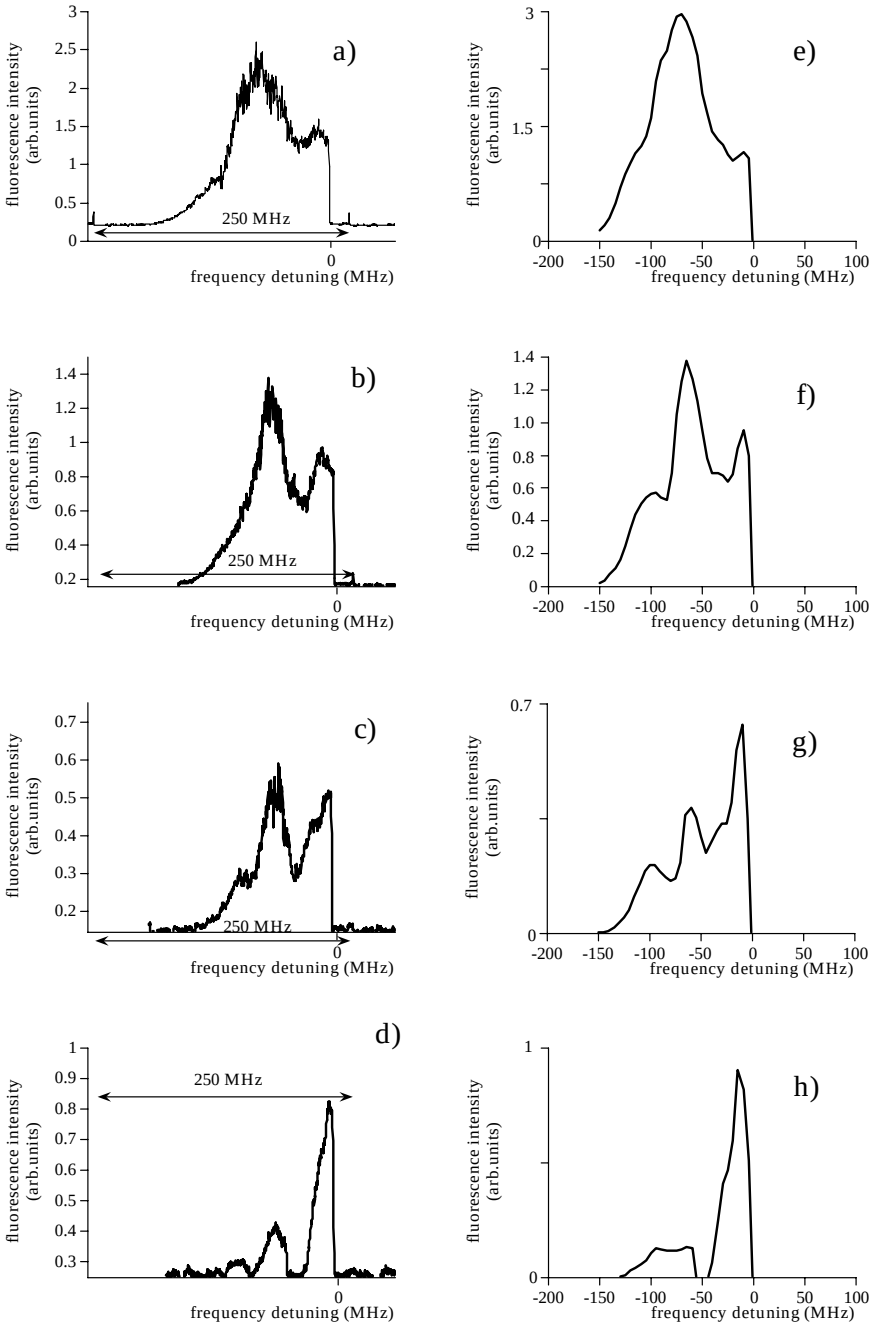

Fig. 4. (a-d) Fluorescence signals of trapped atoms as a function of the TL frequency for the RL tuned to the D_2, $F = 1 \rightarrow F' = 2$ transition. The TL and RL total powers are equal and their value is: (a) $I = 120$ mW; (b) $I = 60$ mW; (c) $I = 30$ mW; (d) $I = 15$ mW; (e-h) fluorescence signal according to the model simulation, calculated upon the corresponding conditions.

A more detailed analysis shows that by suitably tuning the RL, the separation between the two peaks may disappear and a continuous trapping is achieved as shown in Figure 4. The signals correspond to decreasing laser intensities. Each of them is compared with the model calculation and once more a good agreement is obtained. When the laser intensities are about 120 mW (Fig. 4a), a very bright spot is observed inside the cell and its intensity changes with the TL frequency. Three poorly resolved peaks can be observed in Figure 4a. From the right side, the first two peaks correspond to trap I and trap II. The weakest peak (more evident at weaker intensities, see Figs. 4c and 4d) is instead due to the $F = 2 \rightarrow F' = 1$ level and, as long as we know, it has not been reported before. By decreasing the laser intensities, the signal amplitudes decrease as well, and the three peaks get more and

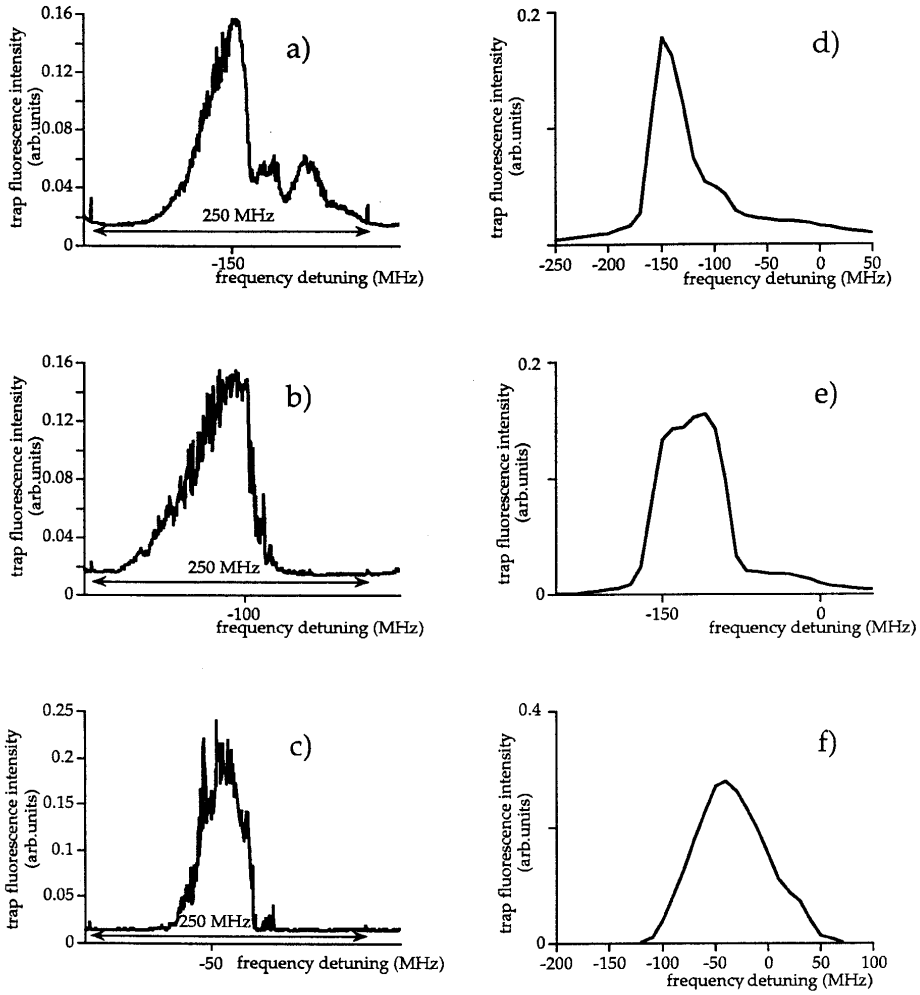

Fig. 5. (a-c) Fluorescence signals of trapped atoms as a function of the repumping laser frequency and for different trapping laser frequencies. Both lasers are tuned to the D_2 line, and they have the same power ($I_{TL} = I_{RL} = 120$ mW). (a) ν_{TL} is red detuned by 10 MHz with respect to transition D_2, $F = 2 \rightarrow F' = 3$: $\Delta\nu_{TL}^{2\rightarrow 3} \cong +10$ MHz; (b) $\Delta\nu_{TL}^{2\rightarrow 3} \cong 30$ MHz; (c) $\Delta\nu_{TL}^{2\rightarrow 3} \cong 110$ MHz; (d-f) model simulations obtained for the corresponding conditions.

more resolved. At the weakest laser intensities the three peaks are well separated. It is interesting to remark that the peak corresponding to trap II decreases much faster than that of trap I. Once more, all these features are well reproduced by the model.

3.3 Frequency scan of the Repumping Laser

In Figure 5 the MOT fluorescence signals and the model simulations obtained by scanning the repumping laser frequency are reported for different trapping laser frequency tunings. Both RL and TL are tuned to the D_2 transition. TL and RL are on resonance with transitions starting from the $F = 2$ and the $F = 1$ levels of the ground state, respectively. The laser power is 120 mW for both lasers. Interesting and meaningful signals are obtained also in this case where trapping is present for a wide range of RL detunings. The trapping spectral region spans from about 200 MHz down to 50 MHz depending on the TL detuning. At $\Delta\nu_{TL} \cong -10$ MHz with respect to the $F = 2 \rightarrow F' = 3$, the signal has a total width larger than 200 MHz and it shows a three-peak structure. The strongest and narrowest is at $\Delta\nu_{RL} = -150$ MHz. By increasing the TL detuning, the signal width decreases and its maximum shifts to smaller RL detuning. As clearly results from the figure, all these features are again well reproduced by our simulation, which also allows for a wider and clearer interpretation, like that discussed in the next subsection.

3.4 Two-dimensional map of the trapping regions

In Figure 6 a complete map of trapping region as a function of trapping and repumping laser frequencies obtained with our model is reported. In Figure 6a both lasers are

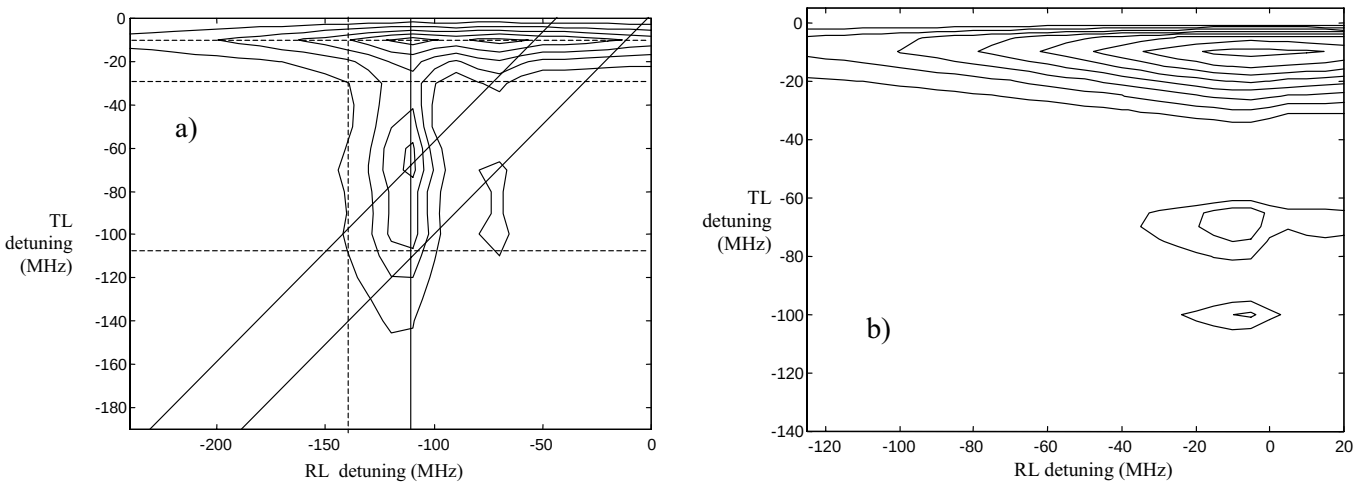

Fig. 6. Map of "trapping regions" as a function of the TL and RL detunings. In (a) both lasers are tuned to the D_2 line. The zero detunings are set to the $F = 2 \rightarrow F' = 3$ and to the $F = 1 \rightarrow F' = 3$ transitions, respectively. The horizontal dashed lines correspond to the conditions of the four RL scans reported in Figure 8. The vertical lines correspond to the TL scans reported in Figure 4 (solid) and in Figure 3 (dashed). The oblique lines represent scans made with a single laser + EOM setup, as *e.g.* in reference [1]. In (b) the TL is tuned to the D_2 line and the RL to the D_1 line. In this case the RL zero detuning is set at the D_1, $F = 1 \rightarrow F' = 2$ resonance.

tuned to the D_2 line. This map allows one to reproduce the fluorescence signals of trapped atoms reported in this present paper as well as in others, *e.g.* [8]. The vertical lines in the figure correspond to the signals reported in Figure 4; the horizontal ones to those shown in Figure 5. The diagonal lines reproduce the signals reported in Figure 3 of reference [8], where the standard apparatus using a single-laser with a side-band repumping frequency makes the trapping and repumping frequencies tuned together.

The role played by the repumping laser is somehow changed when it is resonant with the $P_{1/2}$ level to get the "trap III" conditions, as shown in Figure 7. When the RL is tuned to the D_1 transition and the TL to the D_2 transition respectively, no continuous trapping as a function of the trapping frequency is observed. Actually, in trap III, three peaks are still present but now they are always well resolved. Their dependence of their amplitude on the laser intensity is similar to that reported in Figure 2. The agreement of the computer simulation with experiment is very good. In Figure 6b the trapping map obtained when the TL and the RL are tuned to the D_2 and D_1 lines respectively is shown and the results shown in Figure 7 can be easily reconstructed. In this case he detuning of the laser tuned on the D_1 is referred to the transition D_1, $F = 1 \rightarrow F' = 2$.

4 Discussion

The main features of "type II" and "type III" traps are now clear and the presence of large trapping regions as a function of the TL and RL detunings has been experimentally demonstrated and theoretically modeled. This section is devoted to analyze in some detail the nature of these traps, taking into consideration the force contribution originating from each single transition. In particular, we discuss the reason for which the continuous trapping as a function of the TL frequency scanning may disappear by shifting the repumping laser from the D_2 to the D_1 transition. In order to understand it the forces responsible of trap I, trap II and trap III have to be analyzed in detail. Let us first consider the trapping forces when the RL is tuned to the D_1 transition. The net confinement force acting on the stopped atoms near the trap centre, as a function of the TL detuning has been calculated. This force and the forces due to each optical transition are shown in Figure 8. In this plot, negative values correspond to forces directed to the trap center. Therefore negative values correspond to trapping condition and positive one to expelling condition. The plot of the total force reported in Figure 8b explains in detail the reason for the existence of the three peaks shown in Figure 7, while the single forces separately plotted in Figure 8a allow for a quantitative evaluation of the contribution coming from each transition. For -40 MHz $< \nu_{TL} < 0$, the net force is negative and it is mainly due to the contribution from the D_2, $F = 2 \rightarrow F' = 3$ transition. When $\nu_{TL} \cong -40$ MHz, the force changes its sign and the trap becomes unstable. This is due to the contribution from the D_2, $F = 2 \rightarrow F' = 2$ for which the laser is blue detuned. Note that it is impossible to compensate this force ($F = 2 \rightarrow F' = 2$) by proper choice of the frequency or intensity of the other laser. This is because the $F' = 2$ levels of the $P_{1/2}$ and $P_{3/2}$ states have identical branching ratios to the ground state. Therefore the number of photons absorbed by the $F = 2 \rightarrow F' = 3$ transition should be equal to that absorbed by the D_1, $F = 1 \rightarrow F' = 2$ transition independently on the relation between the intensities of

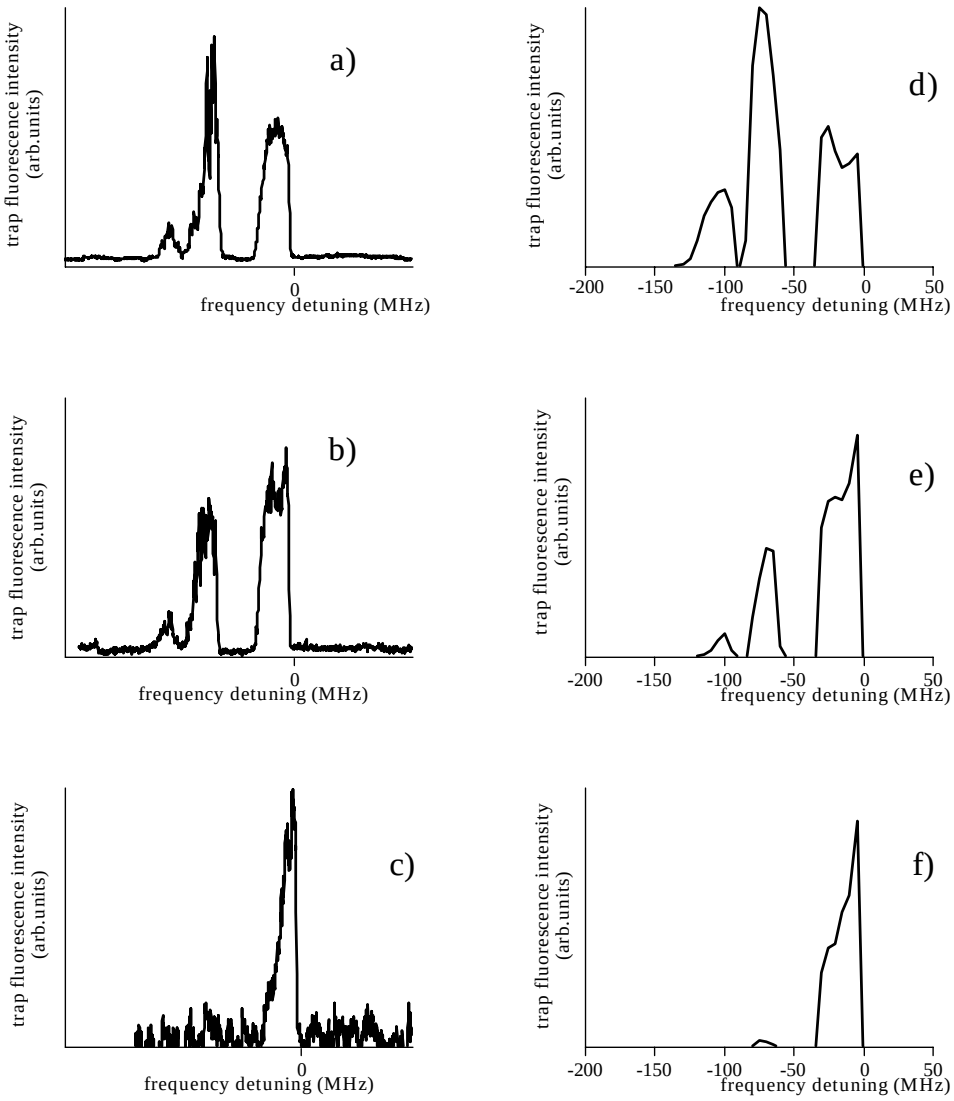

Fig. 7. (a-c) Fluorescence signals from the trapped atoms as a function of the TL frequency for different laser intensities. The TL is tuned to the D_2 line, while the RL is tuned to the D_1, $F = 1 \rightarrow F' = 2$ transition. (a) $I_{\rm TL} = 120$ mW, $I_{\rm RL} = 90$ mW; (b) $I_{\rm TL} = 60$ mW, $I_{\rm RL} = 45$ mW; (c) $I_{\rm TL} = 30$ mW, $I_{\rm RL} = 22.5$ mW; (d-f) fluorescence signals according to model simulations obtained for the corresponding conditions.

the trapping and repumping lasers. For an equal number of absorbed photons on these transitions, the expelling force from the $F = 2 \rightarrow F' = 2$ of the D_2 line is always larger than the force coming from the $F = 1 \rightarrow F' = 2$ of the D_1 line. In fact these forces are determined by the Zeeman splitting of the magnetic sublevels and the Landé factor for the $F'_{\rm P_{3/2}} = 2$ is $g = 2/3$ that is larger than the $g = 1/6$ of the $F'_{\rm P_{1/2}} = 2$ state. This causes the fact that the trap cannot work in the -60 MHz $< \nu_{\rm TL} < -40$ MHz tuning range as demonstrated by the experiment, see *e.g.* the plots reported in Figures 3 and 7.

Let us now evaluate the confinement force when both lasers are resonant with the D_2 transition. In Figure 9 the forces due to the different optical transitions and the total force are reported as a function of the TL detuning. In this case the repumping $F = 1 \rightarrow F' = 0$, 1, 2 transition can compensate the heating force coming from the $F = 2 \rightarrow F' = 2$ transition. This explains why in this case a continuous trapping is possible.

5 Conclusions

The hyperfine structure of the excited levels in alkalis makes necessary a deep analysis of the transitions involved in the cooling and repumping cycles. In particular, the presence in sodium of slightly separated F states makes possible synergetic and competitive effects to come from the two laser frequencies. As these spectral features contribute with large effects in determining the trapping force, detailed models are needed to take into account several phenomena, which can produce quite different behaviors even in similar level structures. In fact, our model

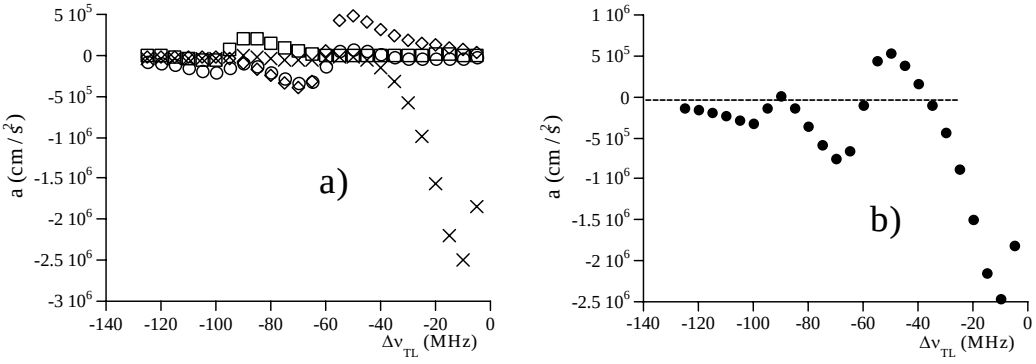

Fig. 8. Radiative force as a function of TL detuning when TL is tuned to the D_2 and RL to the D_1 line respectively. (a) Forces due to single transitions. Contributions of RL ($\circ$) and TL ($\square$) $F = 2 \rightarrow F' = 1$, ($\diamond$) $F = 2 \rightarrow F' = 2$, ($\times$) $F = 2 \rightarrow F' = 3$ are shown. The RL frequency is fixed, and tuned to the D_1, $F = 1 \rightarrow F' = 2$ transition. Its contribution changes during the TL scan, due to the varying pumping effect of this latter; (b) total force as a function of the TL frequency, obtained as a sum of the contributions plotted in (a).

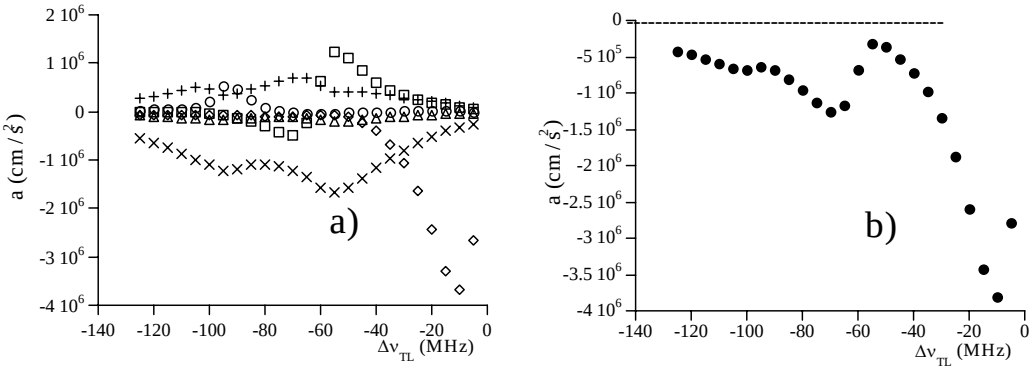

Fig. 9. Radiative forces as a function of TL detuning. Both TL and RL are tuned to the D_2 line. (a) Forces due to single transitions. Contributions of TL on ($\circ$) $F = 2 \rightarrow F' = 1$, ($\square$) $F = 2 \rightarrow F' = 2$, ($\diamond$) $F = 2 \rightarrow F' = 3$ are considered. The RL frequency is fixed and tuned to the D_2, $F = 1 \rightarrow F' = 2$ transition, but its contributions due to ($\times$) $F = 1 \rightarrow F' = 0$, ($+$) $F = 1 \rightarrow F' = 1$, and ($\triangle$) $F = 1 \rightarrow F' = 2$ also change with the TL scan, due to the varying pumping effect of this latter; (b) total force as a function of the TL frequency, obtained as a sum of the contributions plotted in (a).

can be applied to other alkali atoms, provided that their peculiar level structure is considered; in spite of the similarities of many alkali HF structures (number and location of the levels) important differences can be argued, due to the different level separation, Landé factor etc.

Our simulation and our experimental results show that at relatively high laser intensities, both trapping and repumping lasers can actually work as trapping lasers. Moreover there is no preference among $F = 1 \rightarrow F' = 0$, $F = 1 \rightarrow F' = 1$ and $F = 1 \rightarrow F' = 2$ transitions with respect the trapping process when both lasers are tuned on the D_2 line, as instead indicated by Shang *et al.* [8]. Our calculations show that for given atomic velocities the force coming from transition $F = 1 \rightarrow F' = 1$ may be larger than that coming from transition $F = 1 \rightarrow F' = 2$ and that the *vice versa* is possible for other velocities. It is also clear why "type II" trap disappears at low laser intensities but it increases faster than "type I" trap at high intensities; in fact, our simulations show that for trap II, the role of the repumping laser becomes crucial, and its effect increases dramatically with the lasers intensity. The combined action of the two lasers requires that both of them should be on resonance with the same atomic group velocity. However, due to the difference of the g-factor for the hyperfine ground states, the resonance conditions for trapping and repumping lasers vary in the space in a different way and the resonance conditions can be easier fulfilled at higher intensities due to the line broadening.

We would like to acknowledge the technical help of M. Badalassi, S. Bottari, E. Corsi, A. Marchini, A. Pifferi and C. Stanghini. This work has been partially supported by Istituto Nazionale di Fisica Nucleare, Ministero per l'Università e la Ricerca Scientifica e Tecnologica, Università di Siena, Istituto Nazionale di Fisica della Materia.

References

1. E. Raab, M. Prentiss, A. Cable, S. Chu, D. Pritchard, Phys. Rev. Lett. **59**, 2631 (1987).
2. H. Metcalf, P. van der Straten, Phys. Rep. **244**, 203 (1994).
3. J.E. Simsarian, A. Ghosh, G. Gwinner, L.A. Orozco, G.D. Sprouse, P. Voytas, Phys. Rev. Lett. **76**, 3522 (1996).
4. C. Monroe, W. Swann, H. Robinson, C. Wieman, Phys. Rev. Lett. **65**, 1571 (1990).
5. T. Walker, D. Sesko, C. Wieman, Phys. Rev. Lett. **64**, 408 (1990).
6. C.Y. Chen, Y.M. Li, K. Bailey, T.P. O'Connor, L. Young, Z.-T. Lu, to be published.
7. G.D. Sprouse, L.A. Orozco, Ann. Rev. Nucl. Part. Sci. **47**, 429 (1997).
8. S.Q. Shang, Z.-T. Lu, S.J. Freedman, Phys. Rev. A **50**, R4449 (1994).
9. J. Flemming, A.M. Tuboy, D.M.B.P. Milori, L.G. Marcassa, S.C. Zilio, V.S. Bagnato, Opt. Commun. **135**, 269 (1997).
10. K. Molmer, Phys. Rev. A **44**, 5820 (1991).
11. R.S. Williamson III, *Magneto-optical trapping of potassium isotopes*, Ph.D. dissertation, University of Wisconsin, Madison, 1997.
12. K.E. Gibble, S. Kasapi, S. Chu, Opt. Lett. **17**, 526 (1992).
13. K. Lindquist, M. Stephens, C. Wieman, Phys. Rev. A **46**, 4082 (1992).
14. J. Dalibard, C. Cohen-Tannoudji, J. Opt. Soc. Am. B **6**, 2023 (1989).
15. I.I. Sobel'man, *Introduction to the theory of atomic spectra* (Pergamon press, Braunschwaig, 1969).
16. J.D. Louck, Angular momentum theory, in *Atomic, molecular and optical physics handbook*, edited by G.W.F. Drake (American Institute of Physics publishing, New York, 1996); D.A. Varshalovich, A.N. Moskalev, A.N. Khersonskii, *Quantum theory of angular momentum* (Nauka, Moscow, 1975) (in *Russian*).